# Methane C−H Bond Activation by Neutral Lanthanide and Thorium Atoms in the Gas Phase: A Theoretical Prediction

K. J. de Almeida* and A. Cesar

*Departamento de Química, Universidade Federal de Minas Gerais, Avenida Antonio Carlos, 6627, CEP-31270-901, Belo Horizonte, Minas Gerais, Brazil*

*Received February 3, 2006*

Density functional theory (DFT) and Hartree−Fock effective core potential calculations have been performed to investigate the reactivity of neutral f-block atoms toward methane C−H bond activation. The first step of the methane dehydrogenation process, which corresponds to an oxidative insertion, was studied for all lanthanide and actinide thorium atoms. The DFT/B3LYP-correlated results indicate more favorable kinetic and thermochemical conditions for the insertion of the lanthanides with a three non-f valence electron $^2D([f^n]s^2d^1)$ as compared to a two non-f $^1S([f^{n+1}]s^2d^0)$ electronic configuration. Among all the lanthanides, only $^2D([f^n]s^2d^1)$La, Ce, Gd, and Lu may react exergonically with methane; the lowest activation barrier is calculated for La and Ce atoms ($\Delta G^{\ddagger} = 25$ kcal·mol$^{-1}$). A semiquantitative analysis from a simple two-state model shows that an indirect participation of the 4f-orbitals is expected to modify the $[4f^{n+1}]s^2d^0$ reactivity of the Pr, Nb, and Tb−Tm lanthanides as a configuration mixing with the $[4f^n]s^2d^1$ electronic configuration may be quite effective. The most interesting result obtained in this work is for the insertion of the $[5f^0]7s^26d^2$ thorium into the methane C−H bond, where an essentially barrierless ($\Delta G^{\ddagger} = 0.3$ kcal·mol$^{-1}$) and considerably exergonic ($\Delta G = -38$ kcal·mol$^{-1}$) reaction is predicted to occur. The performance of a Th neutral atom overshadows the catalytic power of the best of the lanthanides, Ce, in the $[4f^0]6s^25d^2$ electronic configuration. One of the most important factors for this effectiveness comes from the 5f-orbital radial overlap onto the 7s6d valence shell, which enhances the ability of thorium as a catalyst for methane C−H bond activation.

## Introduction

The effective use of methane as a raw material for industrial applications remains one of the long-standing problems in catalysis. Over the past years, several different direct and indirect routes for the methane conversion to value-added products, such as higher hydrocarbons and oxygenates, have been considered because of the high economical, environmental, and political impact that this process may cause.[1,2] The thermodynamical control of the methane oxidation is one of the greatest challenges found hitherto, since the large amount of energy necessary to activate this molecule, without a catalyst agent, happens to greatly disfavor the stabilization of the intermediary species (alcohol, aldehyde, ketone, etc.) as compared to the most thermodynamically stable products, carbon dioxide and water.[3]

Methane dehydrogenation by bare transition metals (TM) is one of the most common reactions involving a transition element and an alkane in the gas phase. Not surprisingly, great efforts have been spent in the last decade on experimental and theoretical investigations for this type of reaction.[4−28] A direct comparison of the TM reactivity with methane over a wide range of different metals has been essential for screening and understanding the structural, electronic, thermochemical, and kinetic factors that control the energies and the mechanisms of these reactions. The collected data can now be used as valuable guidelines to describe more complex reactions in which a TM and alkane, in particular methane, are the reactants.

* To whom correspondence should be addressed. E-mail: julia@netuno.lcc.ufmg.br.

(1) (a) Rostrup-Nielsen, J. R. *Catal. Today* **2000**, *63*, 159−164. (b) Lunsford, J. H. *Catal. Today* **2000**, *63*, 165−174.

(2) Choudhary, T. V.; Aksoylu, E.; Goodman, D. W. *Catal. Rev.* **2003**, *45*, 151−203.

(3) Labinger, J. A.; Bercaw, J. E. *Nature* **2002**, *417*, 507−514.

(4) Carroll, J. J.; Weisshaar, J. C.; Siegbahn, P. E. M.; Wittborn, C. A. M.; Blomberg, M. R. A. *J. Phys. Chem.* **1995**, *99*, 14388−14396.

(5) Carroll, J. J.; Haug, K. L.; Weisshaar, J. C.; Siegbahn, P. E. M.; Blomberg, M. R. A.; Svensson, M. *J. Phys. Chem.* **1995**, *99*, 13955−13969.

(6) Svensson, M.; Siegbahn, P. E. M.; Blomberg, M. R. A. *J. Am. Chem. Soc.* **1991**, *113*, 7076−7077.

(7) (a) Svensson, M.; Siegbahn, P. E. M.; Blomberg, M. R. A. *J. Phys. Chem.* **1991**, *95*, 4313−4318. (b) Svensson, M.; Siegbahn, P. E. M.; Blomberg, M. R. A. *J. Am. Chem. Soc.* **1992**, *114*, 6095−6102. (c) Svensson, M.; Siegbahn, P. E. M.; Blomberg, M. R. A. *J. Phys. Chem.* **1994**, *98*, 2062−2071.

(8) Wittborn, A. M. C.; Costas, M.; Blomberg, M. R. A.; Siegbahn, P. E. M. *J. Phys. Chem.* **1997**, *107*, 44318−4328.

(9) (a) Ritter, D.; Carroll, J. J.; Weisshaar J. C. *J. Phys. Chem.* **1992**, *96*, 10636−10645. (b) Carroll, J. J.; Weisshaar, J. C. *J. Am. Chem. Soc.* **1993**, *115*, 6962−6968. (c) Carroll, J. J.; Weisshaar, J. C. *J. Phys. Chem.* **1996**, *100*, 12355−12363.

(10) Campbell, M. L. *J. Am. Chem. Soc.* **1997**, *119*, 5984−5985.

(11) Campbell, M. L. *J. Phys. Chem. A* **1997**, *101*, 9377−9381.

(12) Campbell, M. L. *J. Chem. Soc., Faraday Trans.* **1998**, *94*, 353−358.

(13) Campbell, M. L. *Chem. Phys. Lett.* **2002**, *365*, 361−365.

(14) Yang, H.-Q.; Chen, Y.-Q.; Hu, C.-W.; Gong, M.-C.; Hu, H.-R.; Tian, A.-M.; Wong, N.-B. *Chem. Phys. Lett.* **2002**, *355*, 233−240.

(15) Sievers, M. R.; Haynes, C. L.; Chen, Y. M.; Armentrout, P. B. *Int. J. Mass Spectrom.* **2000**, *195*, 149−170.

(16) (a) Chen, Y. M.; Armentrout, P. B. *J. Phys. Chem.* **1995**, *99*, 10775−10779. (b) Chen, Y. M.; Sievers, M. R.; Armentrout, P. B. *Int. J. Mass Spectrom.* **1997**, *167*, 195−212. (c) Liu, F.; Zhang, X. G.; Armentrout, P. B. *J. Phys. Chem.* **2005**, *7*, 1054−1064.

(17) Irikura, K. K.; Beauchamp, J. L. *J. Am. Chem. Soc.* **1991**, *113*, 2769−2770.

(18) Irikura, K. K.; Beauchamp, J. L. *J. Phys. Chem.* **1991**, *95*, 8344−8351.

(19) Buckner, S. W.; McMahon, T. J.; Byrd, G. D.; Freiser, B. S. *Inorg. Chem.* **1989**, *28*, 3511−3518.

(20) Ranasinghe, Y. A.; McMahon, T. J.; Freiser, B. S. *J. Phys. Chem.* **1991**, *95*, 7721−7726.

(21) Simon, A.; MacAleese, L.; Boissel, P.; Maitre, P. *Int. J. Mass Spectrom.* **2002**, *219* 457−473.

10.1021/om060112k CCC: $33.50 
Publication on Web 06/01/2006

In reactivity studies of the 3d, 4d, and 5d family of the TM atoms and ions, it has been observed that both the electron configuration and the spin state of the metallic center are important factors in regulating their gas-phase reactivity and dramatically influence the kinetics of their reactions with alkanes.[4−8] Laser-induced fluorescence experiments have shown that, out of all neutral TMs, only rhodium,[9] palladium,[12] iridium,[10] and platinum[4,6,11,22] can react with methane in the gas phase. From these experiments, termolecular reactions have been observed for Rh, Pd, and Pt atoms, with low-pressure third-order rate constants in the range $10^{-31}$ to $10^{-28}$ molecule$^{-2}$ cm$^6$ s$^{-2}$,[10−12] whereas the reaction between iridium and methane was characterized as a bimolecular process with an activation barrier of 8.8 kcal·mol$^{-1}$.[10] At a temperature of 300 K, platinum ($5d^9 6s^1$[$^3$D]) is the only neutral atom found to react with methane. From another front, the results from quantum chemical calculations employing a parametrized configuration interaction method[4] show that the product of the Pt and $CH_4$ elementary reaction is a collisionally stabilized long-lived $HPtCH_3$ insertion complex rather than the final $H_2$ elimination product.

Most of the TM cations are known to be very reactive toward larger alkanes in general, and a large amount of experimental[14−18,20−22,28] and theoretical[21−24] information is available for the reactivity of these ions with methane, in particular. Within the first row, the complete methane dehydrogenation product is observed only for the early $Sc^+$−$Cr^+$ cations as an endothermic process.[27] Still under endothermic conditions, all second-row TM cations react with methane, yielding molecular hydrogen. More recently, the reaction with $Zr^+$ has been reinvestigated over a wide range of relative kinetic energies that allow both endothermic and exothermic reaction yields to be observed.[28] It was concluded that the $Zr^+/CH_4$ reaction is in fact slightly endothermic and exhibits a strong isotope effect when $CD_4$ is used as reactant. Many third-row TM cations, $Ta^+$, $W^+$, $Os^+$, $Ir^+$, and $Pt^+$, spontaneously dehydrogenate methane, producing the cationic carbene complexes $MCH_2^+$ at room temperature.[18,19]

Gas-phase experiments with lanthanide cations $Ln^+$ (Ln = La−Lu, except Pm, which does not have a stable isotope) and small alkanes and alkenes have disclosed an interesting correlation between the $Ln^+$ reactivity and the stability of the metal excited electronic state having two unpaired non-f electrons.[25] In these studies, it was found that none of the lanthanide cations are able to react with methane, and this inertness has been explained on the grounds of an unfavorable thermochemical formation of the cationic carbene complex $LnCH_2^+$. Early reactivity studies with actinide ions and alkanes or alkenes have mainly focused on the two long-lived actinide elements thorium and uranium.[26,29−32] In a Fourier transform ion cyclotron resonance mass spectrometry investigation, it was shown that only thermalized $Th^+$ ions effectively react with methane to produce a stable gas-phase $ThCH_2^+$ dehydrogenation product.[26]

A great amount of progress has been made for elucidating the mechanisms and the energetic aspects of the reactions between lanthanide organometallic complexes and methane.[33−35] No experimental or theoretical work has been reported yet in the literature dealing with the *neutral* lanthanide atom reactions with alkanes in the gas phase, however. To explore and gain insight into the dependence of the electronic and structural effects on the reactivity of the 4f-block bare elements as catalysts for activating the C−H bond, we have investigated the oxidative insertion of *neutral* lanthanide Ln atoms with methane by means of computational methods.

Three distinct critical points

$$\underset{\mathbf{1}}{Ln + CH_4} \rightarrow \underset{\mathbf{2}}{[HLnCH_3]^{\ddagger}} \rightarrow \underset{\mathbf{3}}{HLnCH_3}$$

located along the insertion reaction path have been analyzed in detail by means of density functional theory and Hartree−Fock methodologies. Above, **1** is a ground or excited electronic state lanthanide atom that reacts with methane to give the transition state complex **2** and then **3**, the metal hydridomethyl product complex of that elementary chemical reaction. According to accepted reaction mechanisms, **3** is the first recognized stable intermediate species occurring on the route to the complete dehydrogenation of methane where a neutral bare metallic center is involved.[4−14,24]

The lanthanide cerium and the actinide thorium atoms show an equivalent propensity to stabilize compounds in a +4 oxidation state in solution phase.[36,37] Hence, Ce ($[4f^0]6s^2 5d^2$) and Th ($[5f^0]7s^2 6d^2$), the parents to Ce(IV) and Th(IV), are expected to have similar catalytic behavior toward the methane C−H bond activation. Motivated by this, and also because of the differentiated performance of the $Th^+$ cation in reacting with methane in the gas phase,[26] computational investigations of the neutral thorium insertion into methane have also been considered in this work for comparative purposes with the analogous Ce + $CH_4$ reaction.

## II. Computational Details

All molecular structures and activation ($\Delta G^{\ddagger}$) and reaction ($\Delta G$) Gibbs free energies were computed at the Hartree−Fock (HF) and density functional theory (DFT) levels. The open-shell calculations were performed using restricted open-shell methods, RO-HF and RO-DFT, and the gradient-corrected hybrid B3LYP functional, which combines Becke's[38] exchange term and the Lee, Yang, and Parr correlation[39] contributions, was employed for the correlated calculations. No higher molecular symmetry restriction has been

(22) (a) Heinemann, C.; Wesendrup, R.; Schwarz, H. *Chem. Phys. Lett.* **1995**, *39*, 75−83. (b) Achatz, U.; Beyer, M.; Joos, S.; Fox, B. S.; Niedner-Schatteburg, G.; Bondybey, V. E. *J. Phys. Chem. A* **1999**, *103*, 8200−8206. (c) Zhang, X. G.; Liyanage, R.; Armentrout, P. B. *J. Am. Chem. Soc.* **2001**, *123*, 5563−5575.

(23) (a) Blomberg, M. R. A.; Siegbahn, P. E. M.; Svensson, M. *J. Phys. Chem.* **1994**, *98*, 2062−2071. (b) Pavlov, M.; Blomberg, M. R. A.; Siegbahn, P. E. M.; Wesendrup, R.; Heinemann, C.; Schwarz, H. *J. Phys. Chem. A* **1997**, *101*, 1567−1579. (c) Westerberg, J.; Blomberg, M. R. A. *J. Phys. Chem. A* **1998**, *102*, 7303−7307.

(24) Zhang, G. B.; Li, S. H.; Jiang, Y. S. *Organometallics* **2003**, *22*, 3820−3830.

(25) Cornehl, H. H.; Heinemann, C.; Schröder, D.; Schwarz, H. *Organometallics* **1995**, *14*, 992−999.

(26) Marçalo, J.; Leal, J. P.; Matos, A. P. *Int. J. Mass Spectrom. Ion Processes* **1996**, *158*, 265−274.

(27) Armentrout, P. B.; Beauchamp, J. L. *Acc. Chem. Res.* **1989**, *22*, 315−231.

(28) Armentrout, P. B.; Sievers, M. R. *J. Phys. Chem. A* **2003**, *107*, 4396−4406.

(29) Gibson, J. K. *Organometallics* **1997**, *16*, 4214−4222.

(30) Gibson, J. K. *Radiochim. Acta* **1999**, *84*, 135−146.

(31) Gibson, J. K. *Int. J. Mass Spectrosc.* **2002**, *214*, 1−21.

(32) Cornehl, H. H.; Wesendrup, R.; Diefenbach, M.; Schwarz, H. *Chem.--Eur. J.* **1997**, *3*, 1083−1090.

(33) Astruc, D. *New J. Chem.* **2005**, *29*, 42−56.

(34) Sherer, E. C.; Cramer, C. J. *Organometallics* **2003**, *22*, 1682−1689.

(35) Maron, L.; Perrin, L.; Eisenstein, O. *J. Chem. Soc., Dalton Trans.* **2002**, *4*, 534−539.

(36) *Comprehensive Inorganic Chemistry*, 1st ed.; Pergamon Press: New York, 1973.

(37) *Advanced Inorganic Chemistry*, 5th ed.; Cotton, F. A., Wilkinson, G., Eds.; John Wiley & Sons: New York, 1988.

(38) (a) Becke, A. D. *Phys. Rev. A* **1988**, *38*, 3098−3100. (b) Becke, A. D. *J. Chem. Phys.* **1993**, *98*, 5648−5652.

(39) Lee, C.; Yang, W.; Parr, R. G. *Phys. Rev.* **1988**, *37B*, 785−789.

imposed at either the electronic wave function or geometry optimization steps; that is, a $C_1$ symmetry point group has been used throughout. After each well-succeeded optimization task, the final molecular structure was then identified as a (relative) minimum energy structure or a first-order saddle point on the potential energy surface by monitoring the numerically calculated harmonic frequencies and their respective vibrational normal modes. The vibrational entropic contribution to the Gibbs free energies and the vibrational zero-point energy (VZPE) corrections were calculated using the harmonic approximation and unscalled vibrational frequencies. The Gibbs free energies were obtained for a temperature of 298.15 K. All calculations were performed employing the GAMESS program.[40]

Quasi-relativistic effective core pseudopotentials (ECP) were used together with both HF and DFT calculations. The treatment of the electronic system in atoms and molecules with ECPs, where some important relativistic effects are built in, is an alternative to a fully relativistic quantum chemistry strategy. A particularly useful scalar ECP developed by the Stuttgart−Dresden group has been employed for all lanthanides atoms.[41,42] This pseudopotential, a large core effective potential (Dolg's LC-ECP), was optimized so that the electrostatic and quasi-relativistic effects of the innermost [Ar]4s4p4d as well as the inner valence 4f-electrons are absorbed into an averaged electrostatic core potential. Hence, only the 5s5p6s5d outer valence shell electrons are explicitly treated in the electron structure calculations. Previous studies[43−45] have demonstrated that the large-core designed ECP calculations are quite suitable for describing the electronic structures of the lanthanide complexes, as the Ln 4f-orbitals are strongly stabilized and remain rather localized in the metal inner valence region. Three types of Dolg's LC-ECP are available.[41,42] The first, Q10 LC-ECP, was optimized for a better description of a lanthanide with 10 electrons in the outer valence shell ($5s^25p^66s^25d^0$) and the $4f^{n+1}$ ($n = 0-13$) inner valence electrons absorbed into the effective core potential; the second, Q11 LC-ECP, was designed for the cases in which 11 electrons are distributed in a $5s^25p^66s^25d^1$ valence subconfiguration and the $4f^n$ ($n = 0-14$) electrons are taken to the core potential; and, finally, Q12 LC-ECP, relevant for calculating the electronic densities of lanthanide atoms in a tetravalent environment, has 12 electrons in a valence $5s^25p^66s^25d^2$ subconfiguration and the remaining $4f^{n-1}$ ($n = 1-14$) electrons are accounted by the core potential.

The issuing of a proper choice for the LC-ECP to be used in the present application hinges to a great extent on the metal ground state electronic configuration, $[4f^n]6s^25d^1$ for La, Ce, Gd, and Lu elements and $[4f^{n+1}]6s^25d^0$ for the remaining lanthanides.[36,37] The electronic configurations of these two subgroups of lanthanide atoms call for using Q11 and Q10 LC-ECPs, respectively. Reciprocally, the low-lying excited state configurations Ln*($[4f^{n+1}]6s^25d^0$) (Ln = La, Ce, Gd, and Lu), and Ln*($[4f^n]6s^25d^1$) (Ln = Pr−Eu, Tb−Yb), obtained by a one-electron 5d → 4f or 4f → 5d transition, are thus suitably described by the Q10 and Q11 large-core ECPs, respectively. In this work, the reactivity of both ground and low-lying excited lanthanide electronic states has been considered. This is because this reaction may take place following a nonadiabatic pathway where the potential energy surfaces of the ground and the 5d ↔ 4f excited states get closer to each other for some particular $Ln/CH_4$ arrangements. Note, however, that only singlet (Q10) or doublet (Q11) spin-coupled electronic states have been considered in the present study. For the calculations involving (triplet spin coupled) Ce ($[4f^0]6s^25d^2$) complexes the Q12 large-core ECP has been used accordingly.

The heavy lanthanide atoms follow a *JJ* rather than a *LS* angular momentum coupling scheme since large electron spin−orbit interactions were present there. It will be assumed however, as a first-order approximation, that the spin−orbit coupling (SOC) energy terms between the $4f^m$ inner-valence and the $6s^p5d^q$ outer-valence subconfigurations are appreciably small,[42,46] and therefore, only a minor error is expected to be introduced in the calculations by ignoring this inner−outer-valence SOC energy contributions. Hence, a frozen $4f^m$ subconfiguration angular moment coupled approximation is assumed for all Ce to Lu lanthanide molecular energy and geometry optimization calculations. Some of the inner−inner spin−orbit interaction contributions are already included in the quasi-relativistic effective LC-ECP.[41,42] No outer−outer SOC correction has been included, however. The effect of the outer−outer SOC on the lantanide valence shell energy separation is estimated to be less than 0.1 eV on the basis of the calculated energy difference between the ground and first excited states of cerocene.[42]

A contracted (7s6p5d)/[5s4p3d] valence double-ζ quality atomic basis set,[41,42] augmented by one f polarization function ($\alpha_f(Ln) = 1.00$) taken from Perrin et al.,[47] was used in conjunction with Dolg's LC-ECP in all lanthanide calculations. A double-ζ 6-31G** atomic basis set[48] plus polarization functions has been used for all carbon and hydrogen atoms with the standard $\alpha_d(C) = 0.8$, $\alpha_p(H) = 1.1$ exponents. For the Ce Q12 calculations, a large C and H triple-ζ 6-311G(2df,2pd) atomic basis set[49] has been employed too.

The structure and electronic energies of the complexes where thorium is the metal center were obtained following a two-step calculation procedure. First, the molecular geometries of the reactants, transition state, and product were fully optimized at the DFT/B3LYP level using the CRENBL pseudopotential[50] and a contracted [5s5p4d3f2g] thorium basis set optimized by Kuechle et al.[51] The CRENBL ECP treats the electronic density of the innermost [Xe]5s5p5d electrons as a core potential, whereas the 12 remaining electrons are explicitly distributed within the 5f6s6p6d7s valence orbitals. The 6-31G** atomic basis set of Pople and coworkers[48] was employed for the C and H atoms. Next, a DFT/B3LYP single-point electronic energy calculation was carried out using an uncontracted primitive (5s, 5p, 4d, 4f) thorium basis set of Christiansen et al.[50] and the carbon and hydrogen triple-ζ 6-311G(2df,2pd) atomic basis set.[49]

## III. Results

**A. Structures. 1. Ln($s^2d^0$) and Ln($s^2d^1$) Complexes.** The optimized structures of all lanthanide hydridomethyl $HLnCH_4$ product complexes (PC) display equivalent atomic arrangements, Figure 1A. The transition states (TS) stabilize, however, in two different molecular conformations, Figure 1B,C. The HF and DFT bond lengths and bond angles are collected in Table 1 and Table 2.

(40) Schmidt, M. W.; Baldridge, K. K.; Boatz, J. A.; Elbert, S. T.; Gordon, M. S.; Jesen, J. H.; Koseki, S.; Matsunaga, N.; Nguyen, K. A.; Su, S. J.; Windus, T. L.; Dupuis, M.; Montgomery, J. A. *J. Comput. Chem.* **1993**, *14*, 1347−1363.

(41) Dolg, M.; Stoll, H.; Savin, A.; Preuss, A. *Theor. Chim. Acta* **1989**, *75*, 173−194.

(42) Dolg, M.; Fulde, P.; Kuchle, W.; Neumann, C. S.; Stoll, H. *J. Chem. Phys.* **1991**, *94*, 3011−3117.

(43) Adamo, C.; Maldivi, P. *J. Phys. Chem. A* **1998**, *102*, 6812−6820.

(44) Dolg, M.; Liu, W.; Kalvoda, S. *Int. J. Quantum Chem.* **2000**, *76*, 359−370.

(45) (a) Maron, L.; Eisenstein, O. *J. Phys. Chem. A* **2000**, *104*, 7140−7143. (b) Maron, L.; Eisenstein, O. *New J. Chem.* **2001**, *25*, 255−258.

(46) In *Encyclopedia of Computational Chemistry (ECC)*; Dolg, M., Ed.; John Wiley & Sons: New York, 1988.

(47) Perrin, L.; Maron, L.; Eisenstein, O. *Inorg. Chem.* **2002**, *41*, 4355−4362.

(48) (a) Hehre, W. J.; Ditchfield, R.; Pople, J. A. *J. Chem. Phys.* **1972**, *56*, 2257. (b) Dill, J. D.; Pople, J. A. *J. Chem. Phys.* **1975**, *62*, 2921−2923.

(49) Krishnan, R.; Binkley, J. S.; Seeger R.; Pople, J. A. *J. Chem. Phys.* **1980**, *72*, 650−654.

(50) Ermler, W. C.; Ross, R. B.; Christiansen, P. A. *Int. J. Quantum Chem.* **1991**, *40*, 829−846.

(51) Kuechle, W.; Dolg, M.; Stoll, H.; Preuss, H. *Mol. Phys.* **1991**, *74*, 1245−1263.

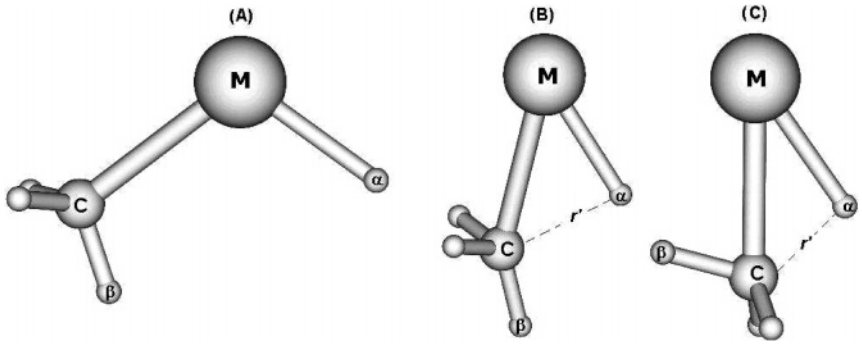


**Figure 1.** DFT/B3LYP-optimized molecular structures of the TS and PC lanthanide hydridomethyl $HLnCH_3$ complexes.

**Table 1. HF and DFT Equilibrium Structural Parameters, Bond Lengths (Å) and Bond Angles (deg), of the Lanthanide Hydridomethyl Product Complexes**

| | | HF | | | DFT | | |
|---|---|---|---|---|---|---|---|
| element | a | Ln−H | Ln−C | ∠H−Ln−C | Ln−H | Ln−C | ∠H−Ln−C |
| La($Z$=57) | $s^2d^1$ | 2.168 | 2.524 | 112.0 | 2.138 | 2.477 | 106.0 |
| Ce($Z$=58) | $s^2d^1$ | 2.150 | 2.503 | 112.5 | 2.111 | 2.455 | 106.2 |
| Gd($Z$=64) | $s^2d^1$ | 2.072 | 2.419 | 114.9 | 2.025 | 2.361 | 108.3 |
| Lu($Z$=71) | $s^2d^1$ | 1.995 | 2.343 | 116.1 | 1.960 | 2.287 | 111.8 |
| Pr($Z$=59) | $s^2d^0$ | 2.318 | 2.657 | 118.9 | 2.243 | 2.582 | 106.7 |
| Nd($Z$=60) | $s^2d^0$ | 2.308 | 2.644 | 119.8 | 2.229 | 2.569 | 107.2 |
| Sm($Z$=62) | $s^2d^0$ | 2.277 | 2.621 | 122.2 | 2.203 | 2.544 | 108.1 |
| Eu($Z$=63) | $s^2d^0$ | 2.267 | 2.612 | 123.8 | 2.193 | 2.534 | 108.9 |
| Tb($Z$=65) | $s^2d^0$ | 2.234 | 2.585 | 126.4 | 2.167 | 2.514 | 111.5 |
| Dy($Z$=66) | $s^2d^0$ | 2.224 | 2.575 | 128.2 | 2.157 | 2.505 | 111.4 |
| Ho($Z$=67) | $s^2d^0$ | 2.212 | 2.564 | 129.8 | 2.147 | 2.496 | 112.2 |
| Er($Z$=68) | $s^2d^0$ | 2.203 | 2.556 | 132.0 | 2.138 | 2.488 | 113.3 |
| Tm($Z$=69) | $s^2d^0$ | 2.195 | 2.550 | 134.6 | 2.131 | 2.483 | 114.4 |
| Yb($Z$=70) | $s^2d^0$ | 2.192 | 2.549 | 137.7 | 2.121 | 2.476 | 115.6 |

[a] Metal ground state electronic configuration.

From Tables 1 and 2, it can be seen that both the uncorrelated and the correlated results give smoothly decreasing Ln−C and Ln−H bond lengths as the respective Ln($s^2d^1$) and Ln($s^2d^0$) series are crossed. This result is caused by the well-known lanthanide contraction effect.[36,37] Our calculations show a DFT (HF) lanthanide contraction $\Delta_X$ (= [$r_{eq}$(La−X) − $r_{eq}$(Lu−X)] (X = C or H)) of $\Delta_C$ = 0.19 Å (0.18 Å) and $\Delta_H$ = 0.17 Å (0.17 Å), respectively. Experimentally, the lanthanide contraction in oxides, halides, and chalcogenides has been measured as 0.179 Å,[52,53] and analogous values, 0.180 and 0.190 Å, have also been obtained for the Ln−N bond in the Ln[$N(SiR_3)_2$]$_3$ compounds by means of MP2 and DFT theoretical calculations, respectively.[47] The Ln−C bond length shrinking effect softens as the metal approches the end of the lanthanide series. One reason for this is that the lanthanide contraction appears to compete with the metal ability to form covalent bonds. This ability, in turn, depends on the $6s^25d^m \rightarrow 6s^15d^{m+1}$ excitation energy that decreases gradually along the lanthanide series and smooths out closer to the end of this series (see next section). Another interesting trend is that the Ln($s^2d^1$) Ln−H and Ln−C bond lengths, in both PC and TS structures, are shorter than the corresponding Ln($s^2d^0$) ones. This may be taken as an indication that more stable Ln($s^2d^1$), as compared to Ln($s^2d^0$), lanthanide complexes are formed.

Regarding the TS and PC ∠H−Ln−C bonding angles, the HF and DFT calculations show that, within each Ln($s^2d^0$)and Ln($s^2d^1$) class of complexes, they become monotonically wide as the lanthanide atomic number increases. In general, the inclusion of the electronic correlation causes a fairly large decrease of about 12°, on average, in the Ln($s^2d^0$) PC H−Ln−C bond angles, whereas for the Ln($s^2d^1$) structures this variation is smaller, 6°, on average. A negligibly small variation is observed in the ∠H−Ln−C angle of the HF and DFT TS structures, however. Compared to each other, the corresponding PC and TS Ln($s^2d^1$) ∠H−Ln−C angles are consistently smaller than those of the Ln($s^2d^0$) class of elements. This result follows from the $\sigma^2$(Ln−C) and $\sigma^2$(Ln−H) valence shell electron repulsion to the SOMO electron left unpaired at the metal center with a Ln($s^2d^1$) atomic configuration, which does not occur within the Ln($s^2d^0$) complexes.

Two different conformations have been optimized for the transition state structures. These TS conformers were readily identified by the single imaginary frequency obtained from a standard vibration normal-mode analysis; only real harmonic frequencies are determined for all optimized PC structures. The imaginary frequency normal mode of both TS structures corresponds to a H−Ln−$CH_3$ bending mode, implying a concerted C−H and M−H bond-breaking and -making motion, respectively. The DFT-calculated imaginary frequencies vary from 1322i to 968i $cm^{-1}$ over the whole lanthanide series. The first structure, Figure 1B, can be described as if the lanthanide atom were approaching perpendicularly to one of the methane tetrahedral faces, while in the second (Figure 1C), the lanthanide is heading toward the methane $H_\alpha$−$H_\beta$ edge along a $C_2$ symmetry axis. In these two cases, an $\eta^3$- or $\eta^2$-like metal−hydrogen interaction arises before the respective TS structures have been reached. The TS complexes then assume two distinct conformations, depending whether the $\eta^3$ or $\eta^2$ frame is involved: a *cis*, Figure 1B, or *trans*, Figure 1C, eclipsed conformer is thus stabilized with respect to the Ln−$H_\alpha$ and C−$H_\beta$ bonds. All PC structures have a *cis* conformation, and therefore, the *cis* TS is qualified to be a late transition state, closer in energy to the respective product complex.

The *cis* TS structure was optimized for all lanthanides regardless of whether the Q10 or Q11 type of LC-ECP is used. The respective torsion angles $\tau$($H_\alpha$LnC−$H_\beta$) are presented in Table 2. The Q10 HF results show a nearly planar $H_\alpha$LnC−$H_\beta$ group ($\tau \approx 0°$), except for the La and Ce TS complexes, while the DFT calculations give a slightly torsioned structure with an average angle of $\tau \approx 10°$, with the largest deviation observed for the Gd and Lu cases. The La and Ce TSs are torsioned structures already at HF calculations, $\tau \approx 25°$, and with inclusion of the electronic correlation, the torsion angle diminishes and stabilizes close to $\tau \approx 15°$.

The cerium TS complexes proved to be a special case since its geometry is rather dependent on the employed LC-ECP and also whether HF or DFT methods are used: a *cis* structure has been optimized at HF and DFT/Q10 as well as at HF/Q11

(52) Shannon, R. D.; Prewitt, C. T. *Acta Crystallogr. B* **1969**, *25*, 925.
(53) Shannon, R. D. *Acta Crystallogr. A* **1976**, *32*, 751−767.

**Table 2. HF and DFT Equilibrium Structural Parameters, Bond Lengths (Å) and Angles (deg), of the Lanthanide Hydridomethyl Transition States[a]**

| | HF | | | | | DFT | | | | |
|---|---|---|---|---|---|---|---|---|---|---|
| element | Ln−H | Ln−C | ∠H−Ln−C | $r'$ | $\tau$ | Ln−H | Ln−C | ∠H−Ln−C | $r'$ | $\tau$ |
| La($Z$=57) | 2.127 | 2.533 | 38.0 | 1.566 | 24.8 | 2.141 | 2.489 | 37.5 | 1.561 | 16.7 |
| Ce($Z$=58) | 2.112 | 2.502 | 38.5 | 1.565 | 24.6 | 2.110 | 2.490 | 36.9 | 1.502 | −13.5 |
| Gd($Z$=64) | 2.050 | 2.387 | 41.9 | 1.618 | 1.5 | 2.041 | 2.380 | 41.7 | 1.607 | 22.3 |
| Lu($Z$=71) | 2.015 | 2.693 | 41.5 | 1.786 | 0.0 | 1.976 | 2.346 | 46.4 | 1.736 | 24.4 |
| Pr($Z$=59) | 2.256 | 2.513 | 46.6 | 1.900 | 0.1 | 2.225 | 2.488 | 47.7 | 1.919 | 10.8 |
| Nd($Z$=60) | 2.239 | 2.497 | 47.3 | 1.914 | 0.0 | 2.209 | 2.472 | 48.6 | 1.939 | 9.9 |
| Sm($Z$=62) | 2.206 | 2.474 | 48.6 | 1.942 | 0.0 | 2.176 | 2.448 | 50.2 | 1.978 | 9.2 |
| Eu($Z$=63) | 2.192 | 2.468 | 49.3 | 1.960 | 0.1 | 2.162 | 2.441 | 51.2 | 2.003 | 8.8 |
| Tb($Z$=65) | 2.160 | 2.445 | 50.7 | 1.989 | 0.0 | 2.133 | 2.420 | 53.0 | 2.049 | 8.3 |
| Dy($Z$=66) | 2.146 | 2.439 | 51.4 | 2.006 | 0.1 | 2.118 | 2.416 | 53.9 | 2.073 | 8.5 |
| Ho($Z$=67) | 2.132 | 2.432 | 52.1 | 2.022 | 0.2 | 2.104 | 2.412 | 54.8 | 2.097 | 8.3 |
| Er($Z$=68) | 2.120 | 2.428 | 52.8 | 2.041 | 0.2 | 2.091 | 2.411 | 55.8 | 2.124 | 8.2 |
| Tm($Z$=69) | 2.108 | 2.426 | 53.5 | 2.060 | 0.0 | 2.078 | 2.409 | 56.7 | 2.151 | 8.2 |
| Yb($Z$=70) | 2.099 | 2.423 | 54.2 | 2.086 | 0.2 | 2.067 | 2.409 | 57.6 | 2.186 | 7.4 |

[a] $r'$ is the C−$H_\alpha$ distance, as in Figure 1B, and $\tau$ is the $H_\alpha$LnC−$H_\beta$ torsion angle.

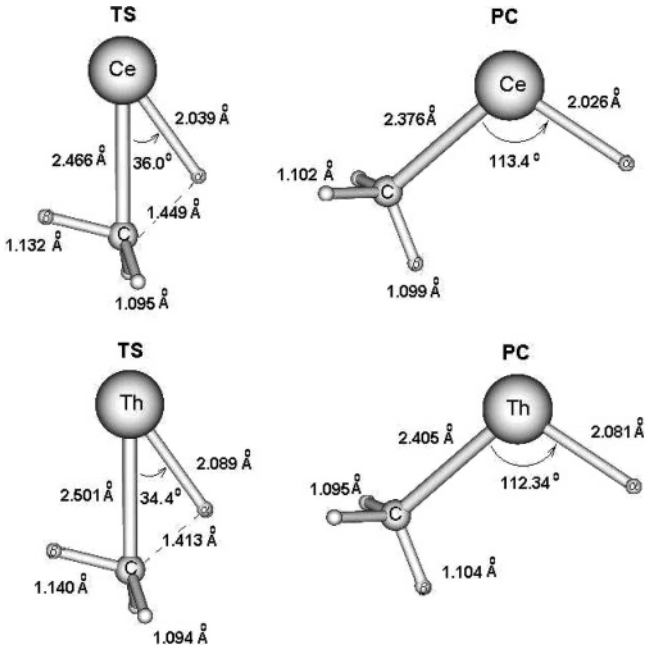


**Figure 2.** DFT/B3LYP equilibrium bond lengths and bond angles of the TS and PC cerium (Q12 LC-ECP) and thorium hydridomethyl complexes.

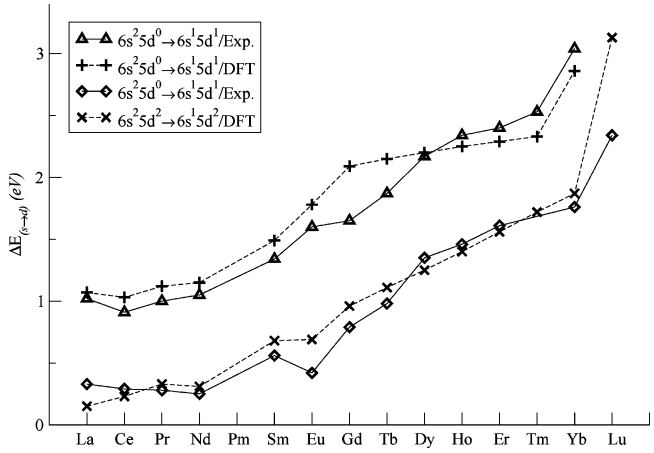


**Figure 3.** Experimental and DFT $[f^{n+1}]6s^25d^0(^1S) \rightarrow [f^{n+1}]$-$6s^15d^1(^3D)$ and $[f^n]6s^25d^1(^2D) \rightarrow [f^n]6s^15d^2(^4F)$ lanthanide atomic excitation energies (in eV).

calculations, whereas a *trans* conformation has been obtained at the DFT/Q11 level. A *trans* conformation is also optimized for DFT and HF methods using a Q12 LC-ECP. The DFT Q12 and Q11 cerium *trans* TS structures differ from each other in that the $H_\alpha$LnC−$H_\beta$ group in the latter is almost planar with a calculated torsion angle $\tau = -1°$.

**2. Ce($s^2d^2$) and Th($s^2d^2$) Complexes.** The DFT structure results for the $s^2d^2$ valence isoelectronic Ce and Th PC and TS are shown in Figure 2. Q12 LC-ECP has been used for these electronic calculations. From there, it can be seen that the TS and PC/Q12 Ce−H bond lengths are shorter by about 0.1 Å than those obtained from the corresponding Q11 calculation, whereas the Q12/DFT PC bond angle is about 7° larger than that obtained using Q11 LC-ECP. The choice for the different forms of the LC-ECPs plays only a minor role in the calculated $r$(Ce−H), $r$(Ce−C), and ∠H−Ce−$CH_3$ geometric parameters of the Ce complexes.

The DFT/B3LYP calculations give Th PC and TS structures equivalent to those found for Ce Q12 complexes; only slightly larger bond lengths and close bond angles are observed for the thorium complexes. The thorium TS HF structure stabilizes in a *trans* planar conformation, $\tau = 180°$, more symmetric therefore than that obtained for the corresponding cerium TS Q12 geometry. The inclusion of the correlation energy shifts the torsion angle to $\tau = 174°$. Finally, a DFT harmonic frequency of 1170i $cm^{-1}$ (1166i $cm^{-1}$) has been calculated for the thorium (cerium Q12) TS structure.

**B. Atomic Excitation Energies.** The lanthanide atomic s → d excitation energies $\Delta E^{at}$(sd) have been calculated using both Q10 and Q11 LC-ECP and DFT/B3LYP methods. These energies can be used as a useful electronic parameter to monitor the quality of the theoretical predictions of the neutral lanthanide atom reaction energies and, consequently, their reactivity toward the inert methane C−H bond. The obtained results are shown in Figure 3, where an error bar of about 0.1 eV is estimated for both $s^2d^0 \rightarrow s^1d^1$ and $s^2d^1 \rightarrow s^1d^2$DFT excitation energies.

We note first that the experimental $[f^n]s^2d^1 \rightarrow [f^n]s^1d^2$ excitation energies[54] are remarkably lower than the corresponding $[f^{n+1}]s^2d^0 \rightarrow [f^{n+1}]s^1d^1$ ones, a result that is fully accounted for by the DFT calculations. This feature follows from a partial compensation of the lost $s^2$ closed-shell pairing energy, as the $6s^25d^1 \rightarrow 6s^15d^2$ transition takes place, by the stabilized triplet $d^2$ subconfiguration, a compensation that does not find a mirror in the $6s^25d^0 \rightarrow 6s^15d^1$ electronic transition. Next, the B3LYP/Q10 LC-ECP method overestimates the experimental $[f^{n+1}]s^2d^0$

(54) Martin, W. C.; Zalubas, R.; Hagan, L. Atomic energy levels−the rare earth elements. NSRDS-NBS, National Bureau of Standards, U.S. Dept. of Commerce.

**Table 3. DFT/B3LYP Activation Barriers and Reaction Energies (kcal·mol$^{-1}$) for the Insertion Reaction of Bare Q10 and Q11 Lanthanide Elements into a Methane C−H Bond[a]**

| | Q10 | | | | Q11 | | | |
|---|---|---|---|---|---|---|---|---|
| Ln | $\Delta E_{VZPE}$ | $\Delta G$ | $\Delta E^{\ddagger}_{VZPE}$ | $\Delta G^{\ddagger}$ | $\Delta E_{VZPE}$ | $\Delta G$ | $\Delta E^{\ddagger}_{VZPE}$ | $\Delta G^{\ddagger}$ |
| La | 14.71 | 16.94 | 49.38 | 52.40 | −18.79 | −14.75 | 20.63 | 25.20 |
| Ce | 15.96 | 18.22 | 50.77 | 53.83 | −18.65 | −14.64 | 21.17 | 25.84 |
| Pr | 16.85 | 19.14 | 51.92 | 54.97 | −18.06 | −14.04 | 21.80 | 26.49 |
| Nd | 18.46 | 20.76 | 53.72 | 56.75 | −17.37 | −13.33 | 22.59 | 27.26 |
| Sm | 21.38 | 23.72 | 57.31 | 60.33 | −16.13 | −12.04 | 24.10 | 28.80 |
| Eu | 23.04 | 25.39 | 59.44 | 62.45 | −15.54 | −11.42 | 24.87 | 29.56 |
| Gd | 24.36 | 26.75 | 61.23 | 64.27 | −15.57 | −11.45 | 25.74 | 30.42 |
| Tb | 25.80 | 28.22 | 63.26 | 66.32 | −14.60 | −10.46 | 25.99 | 30.69 |
| Dy | 27.19 | 29.62 | 65.21 | 68.30 | −14.33 | −10.21 | 26.28 | 31.03 |
| Ho | 28.54 | 30.99 | 67.11 | 70.21 | −14.36 | −10.10 | 26.36 | 31.05 |
| Er | 29.85 | 32.32 | 68.99 | 72.10 | −14.29 | −10.11 | 26.22 | 31.15 |
| Tm | 31.04 | 33.51 | 70.68 | 73.80 | −14.38 | −9.98 | 26.39 | 31.11 |
| Yb | 32.25 | 34.72 | 72.33 | 75.43 | −14.08 | −9.45 | 25.80 | 30.71 |
| Lu | | | | | −13.93 | −9.71 | 27.89 | 32.62 |

[a] $\Delta E_{VZPE}$ and $\Delta E_{VZPE}^{\ddagger}$ are the electronic energies corrected by the respective harmonic vibrational zero-point energies

→ [f$^{n+1}$]s$^1$d$^1$excitation energies for the set of atoms running from La to Dy and underestimates them thereafter, Ho to Yb. Overall, an average error of about 10% is obtained, with the largest deviation of 30% observed for the Gd excitation energy. Regarding the [f$^n$]s$^2$d$^1$ → [f$^n$]s$^1$d$^2$ transition (Q11 LC-ECP has been used), the calculated excitation energies oscillate a little close to the experimental values. A larger average error of about 20% is obtained now, with the largest deviation found for La (55%) and Eu (65%) atoms. These apparently poor results arise because of the relatively small s$^2$d$^1$ → s$^1$d$^2$ excitation energies that would probably require a bit more computational efforts and perhaps more accurate electronic structure methods to be better reproduced. It should be noted that the calculated energies are better interpreted as an average over all possible *J*-states of a given electronic configuration, whereas the experimental energies were taken as the lowest *J*-state energy of that configuration. Typically, the experimental energy difference between the lowest and averaged *J*-levels of a lanthanide electronic configuration is about 1200−2000 cm$^{-1}$ (0.15−0.25 eV).[54]

**C. Reaction and Activation Gibbs Free Energies.** The DFT-calculated reaction $\Delta G$ and activation $\Delta G^{\ddagger}$ free energies of all neutral lanthanide atoms with methane are displayed in Table 3 and Figure 4. The HF results are also included in this figure. These energies were obtained using both Q10 and Q11 LC-ECPs so that the reactivity of the lanthanide atoms at their ground and f → d or d → f electronic excited states could be investigated. The vibrational zero-point energy (VZPE) correction amounts to a nearly constant −6 kcal·mol$^{-1}$ for all lanthanides, and it almost cancels out the $-T\Delta S$ entropic correction, which gives another ca. +5 kcal·mol$^{-1}$ energy contribution at 273.15 K.

Starting from the [4f$^{n+1}$]6s$^2$5d$^0$ Q10 large-core results, Figure 4, the HF $\Delta G$ insertion energies are computed to be endergonic whatever the considered lanthanide. These energies rise linearly across the lanthanide series with a total spreading of about 20 kcal·mol$^{-1}$. The Q10 Yb complexes show a seemingly anomalous HF free-energy value probably owing to the more stable closed-shell [4f$^{14}$]6s$^2$5d$^0$ Yb atomic electronic configuration. An analogous trend can be seen from the experimental s$^2$ → s$^1$d$^1$ atomic excitation energies of the f$^{n+1}$ lanthanide subconfiguration.[41,54] As the DFT electron correlation is included, the metal sd hybridization becomes better represented at the molecular field, and this improves a bit the calculated reaction and activation free energies; as a consequence, both $\Delta G$(HYbCH$_3$)and $\Delta G^{\ddagger}$(HYbCH$_3$) fit the general free-energies pattern displayed by the whole lanthanide series.

Differently from the Q10 case, the [4f$^n$]6s$^2$5d$^1$ results predict exergonic reactions ($\Delta G < 0$) for all lanthanides irrespective of whether the HF or DFT methods are used. From Figure 4, the HF free energies are observed to be nearly constant, around −3 kcal·mol$^{-1}$, and for La to Gd and from there, they decrease linearly, reaching a value of −9 kcal·mol$^{-1}$ for Lu. The DFT $\Delta G$ values, however, increase gradually from −15 kcal·mol$^{-1}$, for La, up to −10 kcal·mol$^{-1}$ for Lu. These distinct trends for the HF and DFT results are interpreted as caused by the dynamical correlation contribution, mainly arising from the s$^1$d$^2$ and s$^2$d$^1$ configuration mixing, which is necessary for the early lanthanide atoms (lower 6s$^2$5d$^1$ → 6s$^1$5d$^2$ excitation energy) and

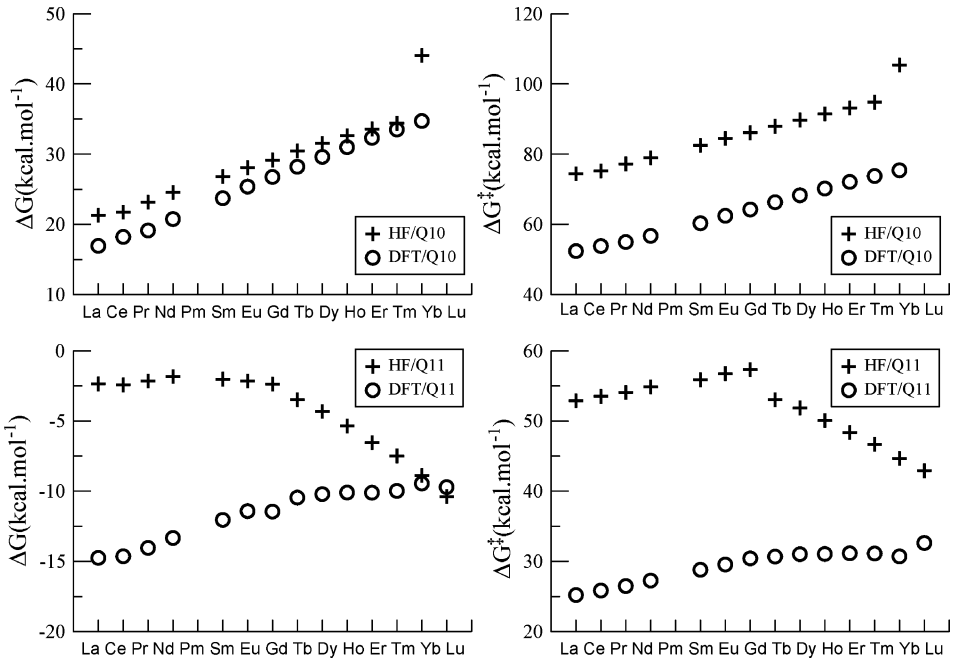


**Figure 4.** HF and DFT/B3LYP activation barriers and reaction energies (kcal·mol$^{-1}$) for the insertion of all Q10 and Q11 lanthanide elements into a methane C−H bond.

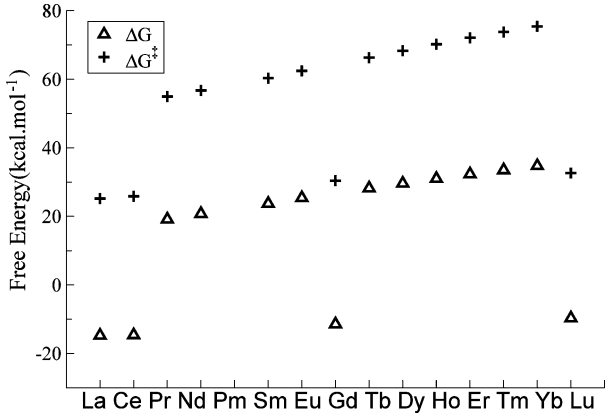


**Figure 5.** DFT/B3LYP $[4f^n]6s^25d^1$ (La, Ce, Gd, Lu) and $[4f^{n+1}]6s^25d^0$ (Pr−Eu, Tb−Yb) lanthanide/methane ground state activation and reaction free energies.

decreases in importance for the late lanthanides (larger $6s^25d^1 \rightarrow 6s^15d^2$ excitation energies). For Yb and Lu atoms, the DFT and HF results are nearly coincident.

In Table 3 and Figure 4 are also collected the calculated $\Delta G^{\ddagger}$ free energies for all neutral lanthanide atoms. As it can be seen, the HF calculations give substantial energy barries, $\Delta G^{\ddagger} > 70$ kcal·mol$^{-1}$, for all $s^2d^0$ atoms with values rising linearly along the whole series. A net energy variation of about 30 kcal·mol$^{-1}$ is obtained as the lanthanide series varies from La to Tm. The inclusion of the electronic correlation energy proves to be rather considerable on evaluating the Q10 activation energies: a nearly constant reduction of about 20 kcal·mol$^{-1}$ is observed for each TS along the lanthanide series. As for the Q10 case, the HF Q11 energy barriers increase with a slow rate from 53 kcal·mol$^{-1}$ (La) to 57 kcal·mol$^{-1}$ (Gd), and then they decrease gradually to 43 kcal·mol$^{-1}$ for Lu. This apparent anomaly is however correct by the DFT/B3LYP electronic correlation when the Q11 $\Delta G^{\ddagger}$ activation energies gently slope up from 25 kcal·mol$^{-1}$ to 33 kcal·mol$^{-1}$ along the La−Lu sequence. Clearly, the inclusion of the electron correlation energy is much more important for the $s^2d^1$ (Q11) activation energies than for the $s^2d^0$ (Q10) ground state case. This effect can be traced back to the lower atomic (Q11) Ln ($s^2d^1 \rightarrow s^1d^2$) excitation energies, which will allow the $s^1d^{n+1}$ and $s^2d^n$ electron configuration mixing to take place more effectively at the Q11 than at the Q10 Ln/ $CH_4$ transition state geometries.

Finally, Figure 5 summarizes the DFT *ground state* lanthanide/methane $\Delta G$ and $\Delta G^{\ddagger}$ free energies, viz., $[4f^n]6s^25d^1$ for La, Ce, Gd, Lu and $[4f^{n+1}]6s^25d^0$ for Pr−Eu, Tb−Yb atoms. From there, we can see that the best thermochemical ($\Delta G$) and kinetic ($\Delta G^{\ddagger}$) reaction conditions belong to the $[4f^n]6s^25d^1$ elements. Furthermore, among all neutral lanthanide atoms, the early La and Ce are predicted to be the most effective methane C−H bond activation catalyst agents with an estimated activation energy barrier of 25 kcal·mol$^{-1}$ and a reaction exergonicity of $\Delta G = -16$ kcal·mol$^{-1}$.

## IV. Discussion

The thermochemical and kinetic aspects of the metal insertion into a methane C−H bond depend on the capability of the metal to make reasonably strong covalent bonds to hydrogen and carbon atoms and, consequently, to form a stable hydridomethyl product complex.[55] To accomplish this, the metal has to have a ground or accessible low-lying excited state with

(55) Crabtree, R. H. *Chem. Rev.* **1995**, *95*, 987−1007.

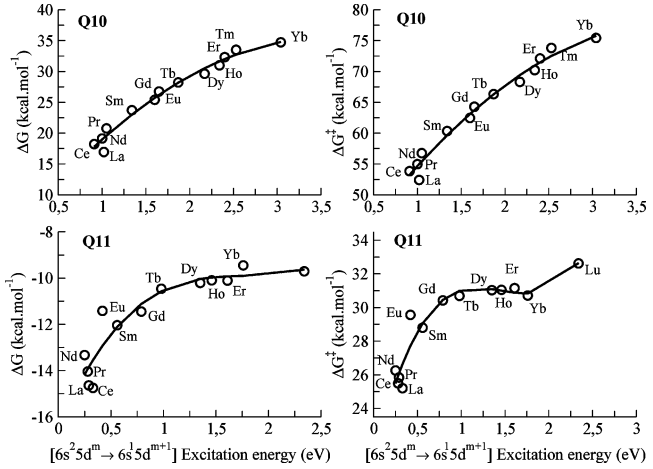


**Figure 6.** Correlation between the experimental $6s^25d^m \rightarrow 6s^15d^{m+1}$, $m = 0$, 1, atomic Ln excitation energies and Q10 and Q11 DFT/B3LYP activation and reaction free energies.

suitable electronic configurations to prompt the metal to make at least two covalent bonds. Given the Ln ground state configurations, $[4f^{n+1}]s^2d^0$ or $[4f^n]s^2d^1$, the energy demand to activate a C−H bond is expected to correlate to the metal valence shell $s^2d^m \rightarrow s^1d^{m+1}$ ($m = 0$, 1) electronic excitation (or hybridization) energy. Incidentally, the incipient $s^1d^{m+1}$ electronic state will also contribute to decrease the energy requirements at the early stage of the activation reaction. This is because the triplet $s^1d^1$ or quartet $s^1d^2$ metal coupled open-shell structures, as compared to the singlet $s^2d^0$ or doublet $s^2d^1$ electronic configurations, will render a smaller electrostatic repulsion interaction as the metal approaches the closed-shell alkane target.

The DFT-calculated $\Delta G$ and $\Delta G^{\ddagger}$ are ploted as a function of the experimental Ln atomic excitation energies in Figure 6. We observe that the reaction and activation free energies, in general, indeed increase with the lanthanide s → d excitation energies, as already anticipated. A rather good quadratic correlation follows between the available experimental Ln $6s^25d^0 \rightarrow 6s^15d^1$ excitation energies[54] and the DFT Q10 $\Delta G$ and $\Delta G^{\ddagger}$ results. Lanthanium ($Z = 57$) appears as the sole exception, having reaction and activation energies slightly lower than those expected from the quadratic correlation curve. An equivalent correlation with the $6s^25d^1 \rightarrow 6s^15d^2$ excitation energies is not exactly obtained for the Q11/DFT free energies, however. Particularly, a slight oscillation is observed for the early lanthanides, from La to Sm, and a flat line is found for the remaining atoms.

The DFT/B3LYP-driven forces $\Delta G^{\ddagger}$ and $\Delta G$ point out that the lanthanide atoms with a three valence non-f electron configuration $[f^n]s^2d^1$ clearly favor kinetic and thermodynamically the methane activation over the case where the metal has a two non-f valence electron $[f^{n+1}]s^2d^0$ configuration. Two main electronic factors contribute to the improved Ln ($[f^n]s^2d^1$) reactivity: (1) the energy required to make a $[f^n]s^2d^1 \rightarrow [f^n]s^1d^2$ electronic transition is lower than the corresponding $[f^n]s^2d^0 \rightarrow [f^n]s^1d^1$ transition, as seen in section 3.2, and (2) a priori, methane undergoes an oxidative insertion only with electron-rich metallic centers. The former factor makes it more facile to the metal to form two covalent bonds within the $[f^n]s^1d^2$ electronic configuration than the corresponding $[f^{n+1}]s^1d^1$ one. The latter aspect is important because only the metal with free valence electron density larger than that involved in the $\sigma$(M−H) and $\sigma$(M−C) bonds can effectively promote electron back-donation into the methane $\sigma^*$(C−H) antibonding

orbital and, therefore, induce a homolytic C−H bond cleavage. This factor is indeed in the direction to account for a previous experimental result[25] that shows that none of the $Ln^+([f^{n+1}]s^1d^0)$, $Ln^+([f^n]s^1d^1)$, or $Ln^+([f^n]s^0d^2)$ cations react with methane. On the basis of these simple electronic arguments, we may possibly anticipate that the $[f^n]s^2d^1$ or $[f^{n+1}]s^2d^2$ lanthanide negative ions $Ln^-$ would have a much better alkane C−H bond catalyt activity than its neutral or one-electron-stripped positive ion relatives.

The relative contribution of the 4f-orbitals in the chemical bonds of some lanthanide complexes has been the subject of earlier computational investigations.[43−45,56] It has been concluded that the 4f-orbitals do not contribute appreciably either to the bonding or to the antibonding molecular orbitals, and therefore, the lanthanides should form chemical bonds almost exclusively by sharing their 6s5d hybrid atomic orbitals. No investigation on the participation of the 4f electron with a lanthanide TS intermediate structure however has been reported yet. Interesting enough, the 4f-electrons may indirectly[56] contribute to a lanthanide bonding, as these orbitals can alternatively act as an electron reservoir for generating the $[4f^n]6s^25d^1$ configuration from the electronic $[4f^{n+1}]6s^25d^0$ ground state configurations and vice versa. With this possibility, the pair of intertwining f ↔ d electronic states may then play a decisive role in lanthanide chemistry in general. Two complementary cases, among others, immediately emerge for an *indirect* participation of the f-electrons in a lanthanide chemical reaction. First, at the entrance channel, the Boltzmann population of the *atomic* ground and the f ↔ d excited states can be comparable at a given thermal condition such that the Ln/methane reaction will develop following independently the two (ground and excited) potential energy surfaces (PES) with competing or nearly competing probabilities. This will most probably be the case for the lanthanides with relatively small excitation energies, namely, Tb and likely Pr too. Second, along the reaction path, the two f ↔ d electronic states, depending on the colliding atom−molecule system symmetry, may efficiently interact with each other at one or some points of the two adiabatic PESs so that a number of geometric avoided crossing structures will develop there. This is a common feature in a number of gas-phase ion/molecule reactions.[25,57,58]

The occurrence of avoided crossings between the ground and the excited electronic PES surfaces of the $Ln/CH_4$ pair is an indispensable factor for the evaluation of the real catalytic effectiveness of the neutral lanthanide atoms.[25] A semiquantitative screening for the cases where probable PES crossings may occur along the reaction path may be given by a simple two-state model where the $[4f^n]6s^25d^1$ and the intrinsically less reactive $[4f^{n+1}]6s^25d^0$ PESs are considered; see Figure 7. Within this model, a better theoretical description for the $Ln/CH_4$ wave function is expected to be given by a mixed configuration state function (CSF). The use of Q10 and Q11 LC-ECP precludes one however from optimizing a f ↔ d multireference electronic state wave function. Also, because of the different number of electrons explicitly treated in each case, it prevents us from obtaining Q10 $[4f^{n+1}]6s^25d^0$ and Q11 $[4f^n]6s^25d^1$ electronic energies on a common scale. Nevertheless, this can be fixed if two simplifying approximations are fulfilled: (1) the Q10- and Q11-optimized TS (PC) geometries are fairly aligned with each other as indicated by the $r_o$, $r_o^*$ and $r_{eq}^*$, $r_{eq}$ marks in Figure 7, and (2) a constant molecular energy difference,

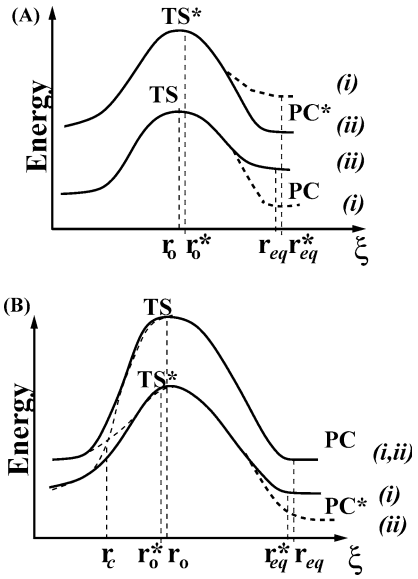


**Figure 7.** Qualitative two-state model along the reaction coordinate ξ for the methane activation by neutral lanthanide atoms (TS transition state and PC product complex): (A) (*i*) La, Ce, and Gd; (*ii*) Sm, Eu, and Yb; (B) (*i*) Nd, Dy−Tm; (*ii*) Pr and Tb.

$$\Delta E^{mol}(f \rightarrow d) = E^{mol}([4f^n]5d^{m+1}) - E^{mol}([4f^{n+1}]5d^m) \approx \Delta E^{atm}(f \rightarrow d);\ n = 0, 13;\ m = 0, 1$$

is maintained throughout the $Ln/CH_4$ reaction path. $\Delta E^{atm}(f \rightarrow d)$ is the $[4f^n]6s^25d^{m+1} \rightarrow [4f^{n+1}]6s^25d^m$ lanthanide atomic excitation energy. The first of these conditions is satisfactorily met, as the Q10- and Q11-optimized $HLnCH_3$ TS (PC) molecular structures are, in fact, quite similar to each other; see Tables 1 and 2. The second requirement is reasonably valid because only a poor overlap is expected between the tightly localized metal 4f and the valence orbitals of the $CH_4$ molecule. According to these approximations, the common scale Gibbs free energies $G'$ and $G'^{\ddagger}$ can be written and the respective free energy differences straightforwardly obtained,

$$\Delta G'(QX) = G(QX) - G_0(QX) = \Delta G(QX)$$

$$\Delta G'^{\ddagger}(QX) = G^{\ddagger}(QX) - G_0(QX) = \Delta G^{\ddagger}(QX)$$

and

$$\Delta G'(QY) = [G(QY) - G_0(QX) + \Delta E^{atm}(f \rightarrow d)]$$

$$\Delta G'^{\ddagger}(QY) = [G^{\ddagger}(QY) - G_0(QX) + \Delta E^{atm}(f \rightarrow d)]$$

QX = Q11 and QY = Q10 applies for the La, Ce, and Gd cases, and the reverse, QX = Q10 and QY = Q11, for the remaining lanthanides. $G_0(QX)$ ($G_0(QX) = G(CH_4) + G[Ln(QX)]$) is the sum of the ground state methane and QX lanthanide atomic free energies. The resulting $\Delta G'$ and $\Delta G^{\ddagger}$ are presented in Table 7 and sketched in Figure 7. Two main conclusions can be drawn from the application, though coarse, of the electronic two-state model of our Q10 and Q11 LC-ECP treatment of the methane activation by a lanthanide atom. First, the C−H bond activation by either the ground or excited states of La, Ce, and Gd as well as Sm, Eu, and Yb group of atoms is predicted to follow along just one unperturbed PES, Figure

(56) Gibson, J. K. *J. Phys. Chem.* **2003**, *107*, 7891−7899.
(57) (a) Van Koppen, P. A. M.; Bowers, M. T.; Fischer, E. R.; Armentrout, P. B. *J. Am. Chem. Soc.* **1994**, *116*, 3780−3791. (b) Koszinowski, K.; Schlangen, M.; Schroder, D.; Schwarz, H. *Int. J. Mass Spectrom.* **2004**, *237*, 19−23.
(58) Perry, J. K.; Ohanessian, G.; Goddard, W. A. *Organometallics* **1994**, *13*, 1870−1877.

**Table 4. Experimental Atomic f → d Lanthanide Excitation Energies and the DFT/B3LYP Common Scale Gibbs Reaction ($\Delta G'$) and Activation ($\Delta G'^{\ddagger}$) Free Energies (in kcal·mol$^{-1}$)[a]**

| | | Q10 | | Q10 | |
|---|---|---|---|---|---|
| element | $\Delta E^{atm}$(f → d) | $\Delta G'$ | $\Delta G'^{\ddagger}$ | $\Delta G'$ | $\Delta G'^{\ddagger}$ |
| | | excited state | | ground state | |
| La | −42.35 | 49.29 | 94.75 | −14.75 | 25.20 |
| Ce | −13.61 | 21.83 | 67.44 | −14.64 | 25.84 |
| Gd | −31.36 | 38.11 | 95.63 | −11.45 | 30.42 |
| | | ground state | | excited state | |
| Pr | 12.68 | 19.14 | 54.97 | −1.36 | 39.17 |
| Nd | 19.37 | 20.76 | 56.75 | 6.04 | 46.63 |
| Sm | 52.35 | 23.72 | 60.33 | 40.31 | 81.15 |
| Eu | 79.56 | 25.39 | 62.45 | 68.14 | 109.17 |
| Tb | 0.92 | 28.22 | 66.32 | −9.54 | 31.61 |
| Dy | 21.68 | 29.62 | 68.30 | 11.47 | 52.71 |
| Ho | 23.98 | 30.99 | 70.21 | 13.88 | 55.03 |
| Er | 20.52 | 32.32 | 72.10 | 10.41 | 51.67 |
| Tm | 37.59 | 33.51 | 73.80 | 27.61 | 68.70 |
| Yb | 66.41 | 34.72 | 75.43 | 56.96 | 97.12 |

[a] The zero energy reference $G_0$(QX) is taken as the sum of the $CH_4$ molecule and lanthanide atom DFT/B3LYP free energies, both at their electronic ground states.

**Table 5. DFT/B3LYP Activation Barriers and Reaction Energies (kcal·mol$^{-1}$) for the Insertion of Ce ([4f$^0$]6s$^2$5d$^2$) and Th ([5f$^0$]7s$^2$6d$^2$) into a Methane C−H Bond[a]**

| element | $\Delta E_{VZPE}$ | $\Delta G$ | $\Delta E_{VZPE}^{\ddagger}$ | $\Delta G^{\ddagger}$ |
|---|---|---|---|---|
| Ce | −30.88 | −27.45 | 8.14 | 10.82 |
| Th | −43.25 | −38.33 | −2.10 | 0.28 |

[a] $\Delta E_{VZPE}$ and $\Delta E_{VZPE}^{\ddagger}$ are the electronic energies corrected by the respective harmonic vibrational zero-point energies.

7A. Therefore, an experimental interpretation and/or an electronic structure calculation using only a single $Ln/CH_4$ electron configuration should be quite appropriate to provide good qualitative and quantitative accounts of the reactivity of these atoms at both the [4f$^{n+1}$]6s$^2$5d$^0$and [4f$^n$]6s$^2$5d$^1$ electronic configurations. On the other hand, the ground and close-lying electronic state PES surfaces for the remaining lanthanides, Pr, Nb, and Tb−Tm, should approach each other, and in the vicinity of the geometry indicated by $r_c$ in Figure 7B, an avoided-crossing structure will develop. Hence, the kinetic and thermodynamical predictions or interpretations of the reaction of these atoms will change quite significantly depending on whether a one- or two-state electronic configuration description is employed. A net activation energy lowering and large changes in the calculated exergonicity of the reactions will result. Necessarily, (at least) a two-state electronic treatment must be used for an accurate representation of these reactions.

**V. Ce ([4f$^0$]6s$^2$5d$^2$) and Th ([5f$^0$]7s$^2$6d$^2$).** In solution phase, the oxidation state IV is quite important for the chemistry of cerium, and it is also the principal oxidation state for the actinide thorium element.[36,37] Because of this resemblance, we may expect a similar gas-phase catalytic behavior of the hot Ce ([4f$^0$]6s$^2$5d$^2$) and Th on activating the methane C−H bond. For the purpose of prospecting a little further in this direction, we have considered the energetic aspects of the reaction of methane with Ce ([4f$^0$]6s$^2$5d$^2$) and Th ([5f$^0$]7s$^2$6d$^2$) neutral atoms. It should be noted that the [f$^0$]s$^2$d$^2$ is the ground state electronic configuration for thorium but a highly excited state configuration for cerium. The results for the Ce (6s$^2$5d$^2$) and Th (7s$^2$6d$^2$) reaction and activation free energies are summarized in Table 5.

First of all, the energies for the Q10, Q11, and Q12 electronic state triad of cerium are useful in verifying the influence of the neutral lanthanide electronic configuration on $CH_4$ activation. The Q12 [4f$^0$]6s$^2$5d$^2$ is predicted to be the most effective of the investigated electronic states of Ce to react with methane: the DFT reaction energy is substantially exergonic, $\Delta G = -28$ kcal·mol$^{-1}$, and the calculated activation barrier is the smallest one, $\Delta G^{\ddagger} = 11$ kcal·mol$^{-1}$, among all the lanthanide atoms. For comparison, the free energies of Ce prepared in the Q10 [4f$^2$]6s$^2$5d$^0$ electronic configuration, $\Delta G = 18$ kcal·mol$^{-1}$ and $\Delta G^{\ddagger} = 54$ kcal·mol$^{-1}$, verify that this atom will hardly be able to react with methane at thermal conditions.

The most striking result for the insertion of a neutral f-block element into the methane C−H bond is for the ground state actinide thorium atom. A fading intermediate TS insertion complex with almost the same energy of the reactants, $\Delta G^{\ddagger} = 0.3$ kcal·mol$^{-1}$, is predicted to give the thorium hydridomethyl product complex in a highly exergonic reaction, $\Delta G = -38$ kcal·mol$^{-1}$. This optimum performance of the neutral thorium atom is interpreted as a consequence of an effective sdf atomic hybridization developed in a molecular environment caused by a strong configuration mixing among the ground [5f$^0$]7s$^2$6d$^2$ and the low-lying [5f$^0$]7s$^1$6d$^3$ and [5f$^1$]7s$^2$6d$^1$ metal excited electronic configurations. Experimentally, the lowest *J* quintet ($^5$F([5f$^0$]7s$^1$6d$^3$)) and triplet ($^3$H([5f$^1$]7s$^2$6d$^1$) and $^3$F([5f$^1$]-7s$^2$6d$^1$)) states corresponding to these electronic configurations lie, respectively, 5563 cm$^{-1}$ (16 kcal·mol$^{-1}$), 7795 cm$^{-1}$ (22 kcal·mol$^{-1}$), and 8243 cm$^{-1}$ (24 kcal·mol$^{-1}$) above the $^3$F([5f$^0$]7s$^2$6d$^2$) ground electronic state.[54] The DFT/B3LYP calculations give 5180 cm$^{-1}$ (15 kcal·mol$^{-1}$) for the first Th [5f$^0$]7s$^2$6d$^2$ → [5f$^0$]7s$^1$6d$^3$ atomic excitation energy. In contrast to the lanthanide elements, where the 4f-orbitals are considerably contracted, the Th 5f-orbitals are relatively spread out close to the outermost 7s and 6d atomic valence orbitals. By inspecting the atomic contributions of the occupied molecular orbitals (MOs) of the TS and PC $HThCH_3$ complexes, a large metal 5f participation in the $\sigma$(Th−H) and $\sigma$(Th−C) bonding valence orbitals is observed. These MOs contain, each, one s$^{0.43}$p$^{0.03}$d$^{0.31}$f$^{0.23}$-hybridized Th atomic orbital.

The lowest DFT/B3LYP activation barriers were found for the $Q12/HCeCH_3$ and $HThCH_3$ complexes, and both have an optimized TS molecular structure stabilized in a *trans* conformation, Figure 2. This indicates that a common molecular precursor is likely formed before the TS structure has been reached. A canditate for this precursor is a weak $\sigma$-bound metal-methane complex with an $\eta^2$-like structure analogous to that inferred from the experimental data for the reactions of rhodium and iridium with alkanes.[59,60] This structure has also been investigated by means of ab initio calculations for several neutral and cation TMs that were found to react with methane.[4,5,58]

To conclude, our results indicate that neutral actinide thorium is a very effective gas-phase catalyst for activating alkanes, and in particular the inert methane. The performance of Th to react with methane overshadows the catalytic power of the best of the lanthanide atoms, the Ce atom in the [4f$^0$]6s$^2$5d$^2$ electronic configuration. This ability comes mainly from the interplay of the 5f-orbital and 7s6d valence orbitals in thorium so that stronger Th−C and Th−H chemical bonds are formed, as previously pointed out by Crabtree.[61] After the $HMCH_3$ intermediate complex **3** has been successfully obtained through the oxidative addition step, a metal-catalyzed $H_2$ reductive elimination sequence will start[4−14] until the methane dehydro-

(59) Periana, R. A.; Bergman, R. G. *J. Am. Chem. Soc.* **1986**, *108*, 7332−7346.
(60) Buchanan, J. M.; Stryker, J. M.; Bergman, R. G. *J. Am. Chem. Soc.* **1986**, *108*, 1537−1550.
(61) Crabtree, R. H. *Chem. Rev.* **1985**, *85*, 245−269.

$$\cdots \rightarrow \underset{HMCH_3}{\mathbf{3}} \rightarrow \underset{[H_2MCH_2]^{\ddagger}}{\mathbf{4}} \rightarrow \underset{H_2MCH_2}{\mathbf{5}} \rightarrow \cdots H_2 + MCH_2$$

genation reaction has been completed. Yet in this case, Th may still be anticipated as a better catalyst agent than any lanthanide atoms since its $[5f^0]7s^26d^2 \leftrightarrow [5f^0]7s^16d^3$ four-electron valence electronic configurations will better stabilize the hydromethylidene intermediate $[H_2ThCH_2]^{\ddagger}$ and $H_2ThCH_2$ complexes.

**Acknowledgment.** K.J.A. acknowledges financial support from Conselho Nacional de Desenvolvimento Científico e Tecnológico (CNPq), Brazil.

OM060112K